A: New Tools and Methods in Experiment and Theory

Crystal Orbital Overlap Population and X-ray Absorption Spectroscopy

Maria Diaz-Lopez, Sergey A. Guda, and Yves Joly

Just Accepted

1
2
3
4
5
6
7
8
9
10
11
12
13
14
15
16
17
18
19
20
21
22
23
24
25
26
27
28
29
30
31
32
33
34
35
36
37
38
39
40
41
42
43
44
45
46
47
48
49
50
51
52
53
54
55
56
57
58
59
60

Crystal Orbital Overlap Population and X-ray Absorption Spectroscopy

Maria Diaz-Lopez,[†] Sergey A. Guda,[§] and Yves Joly*,[¶]

†*ISIS Facility, STFC Rutherford Appleton Laboratory, Didcot OX11 0QX, UK*

‡*Diamond Light Source Ltd., Diamond House, Harwell Science and Innovation Campus, Didcot OX11 0DE, UK*

¶*Univ. Grenoble Alpes, CNRS, Grenoble INP, Institut Néel, 38042 Grenoble, France*

§*The Smart Materials Research Center, Southern Federal University, Sladkova Street 174/28, 344090 Rostov-on-Don, Russia*

∥*Institute for Mathematics, Mechanics, and Computer Science, Southern Federal University, 344090 Rostov-on-Don, Russia*

E-mail: yves.joly@neel.cnrs.fr

Abstract

We present an extension of an *ab initio* numerical tool calculating at the same time x-ray absorption spectroscopies and crystal orbital overlap populations. Density functional theory is used to calculate the electronic structure in both occupied (valence to core X-ray emission spectroscopy) and non occupied states (i.e., X-ray absorption near edge structure, x-ray magnetic circular dichroism) as well as to evaluate the orbital overlap typifying the covalency between neighboring atoms. We show how the different features in the experimental spectra can be correlated to the chemical bonds around the absorbing atoms in several examples including acrylonitrile molecule, rutile TiO_2, Li_2RuO_3 high-energy density cathode, ZnO, and anti-ferromagnetic V_2O_3.

1 Introduction

X-ray absorption spectroscopies are widely used to probe local coordinations with chemical specificity in most classes of materials.[1] Within the energy range close to the absorption edge (≈ 60 eV), X-ray absorption spectroscopies are sensitive to the oxidation state of the absorbing atoms by the resulting edge energy shift compared to a known reference.[2] This sensitivity is even higher when using resonant x-ray diffraction (RXD), as demonstrated by Nazarenko *et al.* for the charge ordering study of magnetite at low temperature.[3] With the exception of strong core-hole interactions observed typically at L_{23} edges of $3d$ elements or M_{45} edges of the rare earth, the absorption cross section and the valence to core x-ray emission spectroscopy are typically proportional to the projection of the non occupied, for the first, and occupied for the second, density of state (pDOS) on the absorbing atom. Thus, a number of studies have used the projection of the non occupied density of states to assign spectral features to specific orbitals, where the atomic orbitals are oftentimes part of a molecular orbital or even a band inside a crystal.

The concept of crystal orbital overlap population (COOP) calculated from the projection of the density of states on a specific molecular bond was developed as a complementary tool to understand interesting aspects of electronic structures.[4–6] COOPs reveal additional bonding information including bonding and antibonding interactions indicated by positive and negative COOP values, respectively. The positive and negative values express respectively the increase or decrease of the electron density in the inter-atomic area by comparison with the electron density which would result from the simple addition of the electron density of both atoms taken as without interaction. As an example of the applicability of COOP to understand the properties of materials, see for example the work from Maintz *et al.* in GeTe phase change material to rationalize the diffusion of Ge in this material.[6] Saubanère and coworkers used COOP calculations to visualize the oxidation of oxygen from oxide to peroxide during the delithiation of a Li_2RuO_3 Li-ion cathode material to RuO_3.[7]

Due to the high complementarity of COOPs with X-ray spectroscopies and pDOS, we

have implemented these calculations in a unified framework: our FDMNES package[8,9]. FDMNES is a self-consistent *ab initio* code, extensively used to simulate XANES, RXD, Surface resonant diffraction, X-ray emission spectroscopy and all related dichroisms including magnetic ones. Its Density Functional Theory (DFT) full potential approach makes this code especially appropriate for simulating absorption edges of chemical elements embedded in non-close packed surroundings or in low symmetry sites, while relativistic calculations including spin-orbit give access to the heaviest chemical elements. The calculations can thus be applied for all classes of materials and it is especially efficient for the K-edge of all elements and the L_{23} edges of the heavy ones (typically $Z \geq 50$).[2] In addition, the scope of the software can be expanded for the calculation of the other edges, while less precisely via a Time Dependent DFT (TDDFT) extension[10]. A recent numerical development[11] allows FDM calculations to be up to 40 times faster than before. This now allows to perform the computation of response functions of diverse materials at reasonable times on conventional personal computers. Our purpose here is also to show that the capabilities of the FDMNES software have been now further expanded to include COOP calculations to aid to the correlation of features in the simulated spectra with the bonding of atoms and ultimately materials properties.

In the next section, the main theoretical elements of the COOP calculation are recalled. Section 2.2 explains how this theory is implemented in FDMNES, particularly in the context of both the multiple scattering theory (MST) and finite difference method (FDM) used in the code to solve electronic structures. Section 3 presents a series of examples where experimental data, simulated spectra, pDOS and the COOP calculations are used to understand the structure-property relationships of a wide range of materials. All the FDMNES input files used for the presented simulations are given in the Supplementary Information.

2 Methods

2.1 Crystal orbital overlap population calculation

For any given calculation mode (MST or FDM), it is possible to make a spherical expansion of the wave function inside an atom A. Considering atom A is spherically symmetric we have:

$$\varphi_A^f \left(\mathbf{r}, \sigma, E \right) = \sum_{L,\sigma} a_{AL\sigma}^f \left(E \right) b_{AL\sigma} \left(E, r_A \right) Y_\ell^m \left(\hat{r}_A \right) \chi_\sigma \ , \tag{1}$$

where $\mathbf{r}$ is the position, $r = |\mathbf{r}|$, $\hat{r} = \mathbf{r}/r$ and σ is the spin. f represents a specific state with energy E, whose definition depends on the basis set used to make the calculation. When neglecting spin-orbit interaction, $L = (\ell, m)$ simply indexes the orbital quantum numbers. $b_{AL\sigma} \left(E, r_A \right)$ is the radial solution of the Schrödinger equation. $\mathbf{r}_A = \mathbf{r} - \mathbf{R}_A$ is the position, relative to the atom A, set at $\mathbf{R}_A$. $a_{AL\sigma}^f$ is the amplitude and χ_σ is the spin projector. Note that the dependence on energy of $b_{AL\sigma}$ is smooth contrary to the one of the amplitudes. We nevertheless keep it because it cannot be neglected all along the wide energy range used typically in absorption spectroscopies. The amplitudes $a_{AL\sigma}^f$ are related to the diagonal, $(L = L')$, pDOS, $\rho_{AL\sigma} \left(E \right)$, by the relation:

$$\rho_{AL\sigma} \left(E \right) = \sum_f \left| a_{AL\sigma}^f \left(E \right) \right|^2 \int b_{AL\sigma}^2 \left(E, r \right) r^2 dr \ , \tag{2}$$

where the radial integration is performed up to a chosen atomic radius.

The COOPs, $\mathcal{C}_{L_A L_B \sigma}^{AB}$, are calculated in the same way, but considering the non-diagonal terms, $(L_A \neq L_B)$:

$$\mathcal{C}_{L_A L_B \sigma}^{AB} \left(E \right) = \mathcal{R}_{L_A L_B \sigma}^{AB} \left(E \right) \sum_f a_{AL_A\sigma}^f \left(E \right) a_{BL_B\sigma}^f \left(E \right) \ , \tag{3}$$

with the integral given by:

$$\mathcal{R}^{AB}_{L_A L_B \sigma}(E) = \int b_{AL_A\sigma}(E, r_A) Y^*_{L_A}(\hat{r}_A) b_{BL_B\sigma}(E, r_B) Y_{L_B}(\hat{r}_B) r^2 dr d\hat{r} \ . \qquad (4)$$

While magnetic system with spin-orbit, $\mathcal{C}^{AB}_{L_A L_B \sigma}(E)$ in Eq. 3 could be a complex number where the imaginary part corresponds to a current, we consider here only contribution of the real part given that the complex conjugate on the harmonics in Eq. 4 are useless when spin-orbit can be neglected. Therefore, real basis for the harmonics are used henceforth.

2.2   COOP in FDMNES

The FDMNES code uses two different techniques to solve the electronic structure: FDM and MST. The FDM applies arbitrarily shaped potentials[12], while full MST gives rise to less precise but faster calculations. Whatever the calculation mode, XANES calculations most often require taking into account core-hole interactions with some screening electrons. Therefore, COOP and pDOS are calculated in the same way (with a core hole) to allow for a direct comparison with the corresponding spectra. The observed effect versus the electronic ground state structure after including core hole effect in COOP and pDOS is mostly a shift and the analysis remains valid. The purpose of this section is to show how these two calculation modes are adapted to the COOP evaluation. We also want to clarify our integration procedure which allows to quantify the orbital overlap. As shown in the last part, it can be expressed in convenient basis, for a better description of the phenomena.

2.2.1   About the integration

FDMNES works in direct space and thus the formulae 3 and 4 can be directly applied, but the practical integration expressed in Eq. 4 needs further clarification. We have chosen to perform the integral in a sphere centered at a point at a relative distance of both atoms equals to the ratio between the two atomic radii. The integration is done in a sphere whose radius is the half sum of both radius. This procedure can be seen as arbitrary, but the important

factor is consistency. Besides the arbitrary assignment of a radius value, and the crude integration step, direct quantitative comparison can be done between COOPs calculations, because when the chemical species do not change, the radius remains the nearly the same. In this way, a quantitative comparison of the COOP between different materials of the same family is possible and metal-ligand bonding can be quantified.

2.2.2 Spin-orbit and full-potential shape

FDMNES calculations can be relativistic with spin-orbit coupling, an important consideration for systems containing heavy atoms as well as for the simulations of x-ray magnetic circular dichroism at K-edges. For relativistic COOP calculations using spin-orbit coupling we use the $L = (\ell, m, s)$ basis instead of the more classical $(\ell, J_{\pm}, J_z)$ basis in relativistic theories, following the work by Wood and Boring[13]. In this model $s = \pm\frac{1}{2}$ is the index of the two solutions of the radial relativistic Schrödinger equation. When spin-orbit tends to zero, s and σ simply merge. Spin-orbit makes also that the radial solution of the Schrödinger equation depends on the four quantum numbers ℓ, m, s and, σ. Their amplitude depends on the same indexes but with the specific form: $a^f_{AL\sigma} = a^f_{A,\ell,m+\sigma-s,s}$. Note that beside these technical difficulties, which must be well resolved in the simulation, a convenient change of basis makes the final extraction of the COOP simpler for the user as explained in section 2.3.

When FDMNES runs in FDM mode a free shape of the potential is assumed and spherical approximation inside the atoms is not used. The use of a sphere with a smaller radius than the one typically used in the muffin-tin approximation is necessary to obtain the spherical expansion given in Eq. 1. Note that an option on the code exists to calculate this area without any spherical approximation. In that case, the wave function can be expressed by an expansion in spherical harmonics using a double sum. Up to now, we have not found cases where this double expansion gives an improvement in the simulations when comparing with experimental spectra. For COOPs, the aspherical components could give

more effects, because the integration in Eq. 4 is performed in the overlapping area where the approximation is suspected to be of a poorer quality. Nevertheless, the general calculation giving the amplitudes, the main "ingredients" of COOPs is in any case correct and only the radial wave functions are slightly less precisely evaluated at these radii. The effect must then be smooth and as it will be demonstrated in the examples below: firstly, we are able to reproduce the COOP results given by other codes; and secondly, we can extract the σ and π bounds in archetypal systems where they are well known.

2.2.3   FDM and MST modes

When using the FDM mode, FDMNES directly solves the (relativistic) Schrödinger equation and furnishes the amplitudes a. On the contrary, when using the MST mode, one gets the multiple scattering amplitudes. When calculating XANES or pDOS we only need the diagonal terms in the atomic expansion ($A=B$). But when using the full multiple scattering, which is inverting the MST matrix and avoiding thus the path expansion, one obtains also the off-diagonal multiple scattering amplitudes, $\tau^{AB}_{L_A L_B \sigma}$. Their expression versus the atomic amplitudes are:

$$\frac{1}{2}\left(\tau^{AB}_{L_A L_B \sigma} - \tau^{BA*}_{L_B L_A \sigma}\right) = \hat{\tau}^{AB}_{L_A L_B \sigma} = -i\sum_f a^f_{A,L_A\sigma} a^f_{B,L_B\sigma} \ . \tag{5}$$

Note that when spin-orbit can be neglected we simply have:

$$\frac{1}{2}\left(\tau^{AB}_{L_A L_B \sigma} - \tau^{BA*}_{L_B L_A \sigma}\right) = i\Im\left(\tau^{AB}_{L_A L_B \sigma}(E)\right) \ . \tag{6}$$

The multiple-scattering amplitudes can be directly inserted in the COOP expression:

$$\mathcal{C}^{AB}_{L_A L_B \sigma}(E) = -\Im\left(\hat{\tau}^{AB}_{L_A L_B \sigma}(E) \mathcal{R}^{AB}_{L_A L_B \sigma}(E)\right) \ . \tag{7}$$

2.3   Choosing the spherical harmonics basis

Different basis for the spherical harmonics can be used. When spin-orbit cannot be neglected, or when calculating electronic structure for punctual group with complex characters (such as C_3 or C_4), the most classical complex spherical harmonics are used and the formulas above are expressed in this way. In the other cases, the tesseral harmonics which are given by the real and imaginary part of the standard harmonics can be preferred to save computing time and memory space. Cubic harmonics which are also real harmonics are the functions corresponding to the cubic punctual group. They are in fact the most familiar and called s, p_x, p_y, p_z, d_{z^2}, $d_{x^2-y^2}$... and can be obtained from the previous ones by very simple matrix transformation. Up to $\ell = 2$ they are the same as the tesseral harmonics, but from $\ell = 3$, they are different. For practical use it is often more convenient to visualize pDOS and COOP using this cubic basis, even when the punctual group is not cubic. We have thus introduced a change of basis and the results are given by default in this way. A specific option in the code allows to keep the standard basis.

The electronic structure is first calculated considering a cluster where the spherical harmonics are expanded in the same (x, y, z) frame. The inter-atomic axis between 2 atoms can be in an arbitrary direction. It is often more convenient to express the COOP in a local basis with the z direction along the inter-atomic axis. In practice this one is chosen automatically depending on the local geometry. This allows to better quantify the bonding with the convenient orbital magnetic quantum number m. Alternatively, the original frame can be selected.

3 Results & Discussion

3.1 Acrylonitrile

More than 20 years ago, Laffon and coworkers[14] performed XANES measurements on acrylonitrile multilayers deposited on Pt(111) and used linear dichroism to compare the spectra recorded at normal (polarization parallel to the surface) and grazing incidence (polarization at 25° from the normal). This study showed the small planar CH_2CHCN molecules are not fully disordered, but mostly parallel between each others at a given angle (not specified in their publication) with the metal surface. With the help of Ultraviolet Photoelectron and infrared spectroscopies,[15] the interpretation of the X-ray spectra in terms of π^* and σ^* bonds was possible. Here, we use this well established result to validate our COOP calculation.

The XANES experimental data and simulation at the Nitrogen K-edge, N p-DOS and COOP between N and C (that we call N:C) are introduced in Figure 1. Note the simulations were done using the FDM approach and are thus full potential, seeing as the muffin-tin approximation is not sufficiently precise in such an open or flat molecule. A single molecule was considered in this calculation with the effect of the neighboring molecules being neglected, but with a constant maximum potential to avoid the slow increase of the potential to zero at infinity, as seen in the gas phase.

Fig. 1 shows experimental and simulated XANES spectra at both polarization conditions. In the inset, a scheme of the molecule with its orientation is given, where the x axis is located along the N-C bond and the z axis is perpendicular to the molecule. A good agreement between the simulation and experiment is achieved, which reproduces the thin and tall features at the lower energy range of the spectra as well at the broader bumps at higher energies. Note that only the pure contributions of the polarization along x, y and z are shown in this study and the average between them to reproduce the data which allows to fit the angle between the molecule plane and the surface can be found in a previous study.[16]. More important for the present study is the replication of different features in the spectra

and their dependance with the polarization direction. Their nature is confirmed both by the N pDOS and the COOP between N and its first neighboring C atom. The pDOS is mostly proportional to the absorption cross section, and we can verify there the concordance between the p_y and p_z N states with the thin XANES features and one of the p_x states with the broader features at higher energy. The assignment of π_z^*, π_y^* and σ_x^* molecular orbitals is possible thanks to COOP simulations. The sign of the features above the last occupied orbital shows the anti-bonding character of the π orbitals, as expected, while the σ orbitals stand in the continuum (so, not bounded to the molecule), and are first bonding then anti-bonding. N-p_x:C-p_x and N-p_x:C-s COOPs in Figure 1 reveal the C-sp_x hybridization.

3.2   TiO$_2$ rutile

Rutile TiO$_2$ with space-group P4$_2$/mnm, is an arrangement of two sets of Jahn-Teller distorted TiO$_6$ octahedron rotated by 90° between them. This compound is an archetypical case to study dipole and quadrupole transitions. Poumellec and co-workers identified these features thanks to linear dichroism experiments.[17] In 1999, we used their data to prove the validity of the FDMNES code[18]. Now, we present the calculation of COOP between Ti $3d$ orbitals and the neighboring p-Oxygen orbitals which are probed by the quadrupolar transitions in XANES.

The comparison between XANES simulations and the data is given in Fig. 2 showing a good agreement for the two polarizations: (0,0,1) and (1,-1,0). For the correct interpretation of the pre-edge features, namely A-C (see Figure 2), a 0.8 electron screening of the core-hole was considered, which produced a convenient shift of the $3d$, e_g and t_{2g} states, by about 2 eV, to observe the quadrupole transition at the A and B peaks, at the pre-edge. B contains also an important contribution of dipole transition. C is only dipole.

In addition to XANES simulations, we calculate COOPs with a focus on the orbitals involving the Ti-$3d$ states including a set of simulations corresponding to a rotation of 45° of the sample around its **c** axis with both polarization and wave vector in the basal (**a**,**b**)
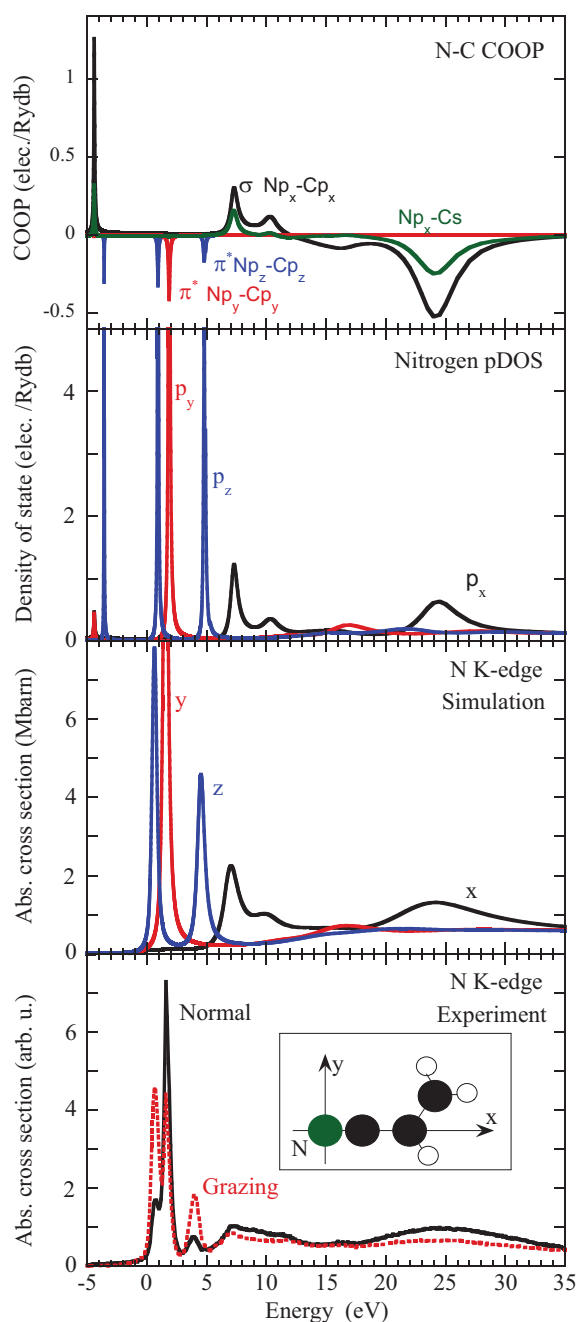
Figure 1: X-ray absorption at the Nitrogen K edge, pDOS and COOP spectra in acrylonitrile. The data recorded at grazing and normal incidences are shown at the bottom with the scheme of the planar molecule and its orientation in the frame given in the inset. The XANES energy scale is shifted to match the simulation zero for the energy set at the Highest Occupied Molecular Orbital. The simulation performed along x, y and z is in good agreement with the experimental data. The N pDOS shows the atomic orbitals involved in the XANES signal. The top figures shows COOP between N and its first C neighboring atom. Bonding (> 0) and anti-bonding (< 0) σ and π molecular orbitals are easy to identify and the connection with the XANES data is straightforward.
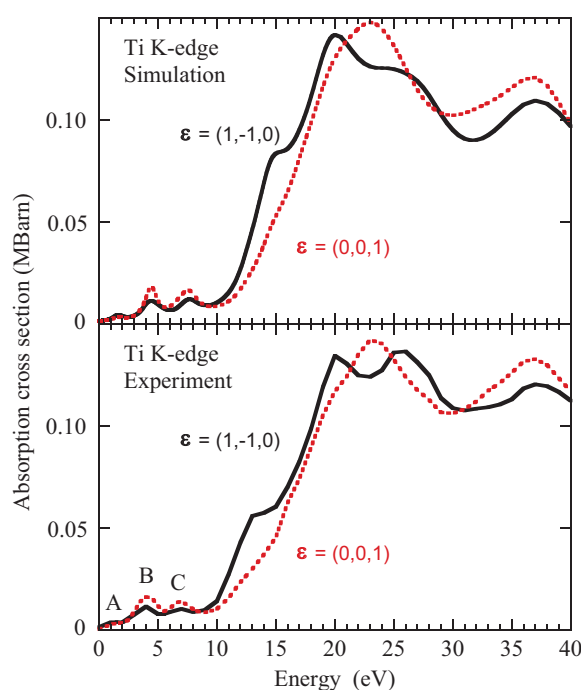
Figure 2: X-ray absorption cross section at the Ti K edge in TiO_2, rutile. Bottom are the data and top the simulation. For all the spectra, the wave vector is along $(1, 1, 0)$. Polarization, dotted: $\epsilon = (0, 0, 1)$, full-line: $\epsilon = (1, -1, 0)$. The agreement is good including at the 3 pre-edge features A, B and C. A is pure quadrupolar, B is mainly dipolar with a contribution of quadrupole, C is dipolar.

plane. As shown in Fig. 3, the (0,1,0) direction does not probe in any way the t_{2g} state at lower energy (pre-edge feature A). This figure shows also the COOPs for Ti-O_1 and Ti-O_2, where Ti-O_2 has the largest inter-atomic distance in the Jahn-Teller distorted octahedron. A figure of the local atomic organization is introduced in the inset of the same figure. In both cases only three COOPs involving the Ti-d and O-p orbitals are non zero for symmetry reason. Using a local z axis along the bond, they are $d_{z2} : p_z$ which is of σ^* anti-bonding type and $d_{xz} : p_x$ and $d_{yz} : p_y$ which are of π^* anti-bonding type. This is indicated by the negative value of the COOP at the B feature for $d_{z2} : p_z$, and the A feature for the 2 others COOPs. Below the Fermi level COOPs are predominantly bonding. Interestingly, we can note that the amplitude of $d_{xz} : p_x$ and $d_{yz} : p_y$ are lower than that of $d_{z2} : p_z$ as expected for a π bond versus a σ bond. Moreover, the $d_{z2} : p_z$ molecular orbital is at higher energy when the Ti-O distance is shorter as it must be for an anti-bonding state. Finally, note that even in an ionic compound, some part of covalency can see in the COOPs. The ionicity is revealed by the amplitudes in the corresponding states, in formula 3, wich is high for Oxygen and low for Ti below the Fermi level, while it is the contrary at positive energy and more specifically for A and B features.

3.3 Li_2RuO_3 and RuO_3

The delithiation of ruthenium oxides is important in the context of Li batteries. Saubanère *et al.*[7] reported the calculation of pDOS and the COOP on Li_2RuO_3 and delithiated compounds in a recent study, which we have used as a test case to compare the calculations performed in real space by FDMNES with the more conventional approach using reciprocal space techniques. As in their study, we have used the Hubbard correction (LDA+U). The structure of Li_2RuO_3 crystallizes in the $C2/c$ space group and consists of interconnected layers of RuO_6 octahedra with C_1 symmetry, that alternate with layers of Li.[19] In the octahedra, all the O-O distances are close to 2.75 Å. The structure contains three non equivalent oxygen sites, and for simplicity we have averaged their response functions in Figure 4. A
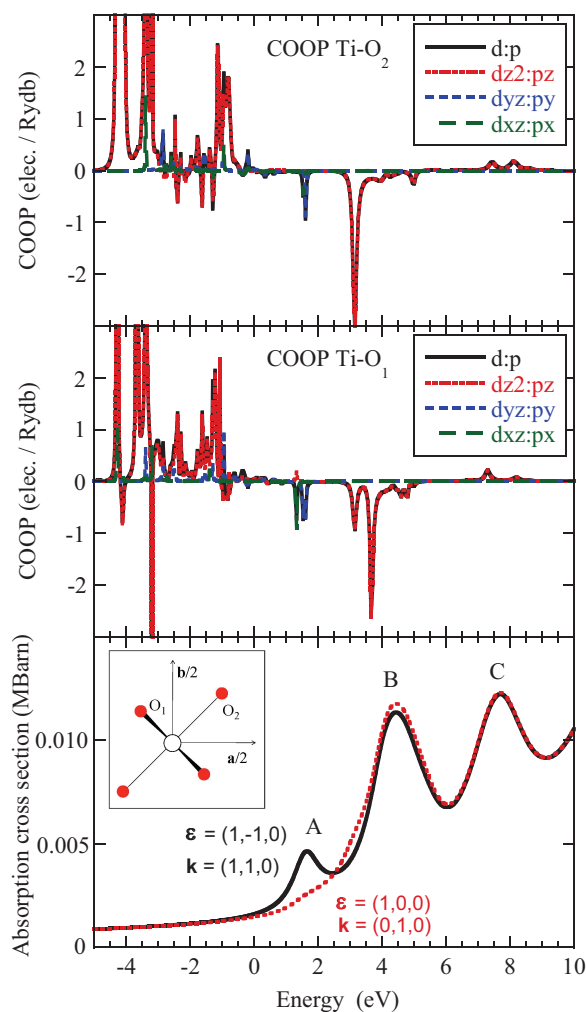
Figure 3: COOP and X-ray absorption spectra at the pre-edge in TiO_2. Bottom is the simulation with two orientations of the sample giving a linear dichroism only for the quadrupole contribution. The local atomic organization with the **a** and **b**, axis of the unit cell is shown in the inset. The local z axis for the COOP is along the Ti-O_i direction with $i = 1$, for the shorter inter-atomic distance and, $i = 2$ for the longer. O_1 is out of the (**a**,**b**) plane. Top and middle figures show the COOP for respectively the Ti-O_1 and Ti-O_2. The $d_{z2} : p_z$ antibonding σ^* molecular level is at higher energy for the shorter inter-atomic distance.

0.1 eV broadening on both COOP and pDOS was applied to allow a comparison with the results of Saubanère *et al.* In spite of the sharper spectral features calculated by FDMNES, comparable COOP and pDOS calculation were obtained. The structure of RuO_3, which crystallizes in the $R\bar{3}$ space group, reported by Akimoto *et al.*[20] was used for the calculations of the delithiated compound. The octahedra in RuO_3, with a C_3 punctual group, is distorted with an shortening of two O-O distances down to 2.36 Å. As stated by Saubanère *et al.* this implies the formation of a O-O bonds in RuO_3 associated to the Li zero occupancy and to a possible reduction of the charge on this O_2 sub-system.

Our simulations are performed using the finite difference method within a 6 Å cluster centered around the Ru atom. They are self-consistent and use the Hubbard parameter U = 5 eV. In Fig. 4 we can see the DOS projected on the Ru and O atoms as well as the COOP between the central atom and its neighbors and between two adjacent oxygen atoms, the closest ones in RuO_3. It is the total pDOS on all valence orbital which is shown but most of the contribution comes from the $4d$ for Ru and $2p$ for O. The pDOS are close to the ones calculated by Saubanère *et al.* despite a 1 eV shift of the Fermi level in Li_2RuO_3. Importantly, we observe the same shift of the main $2p$-O pDOS peak, between Li_2RuO_3 and RuO_3 toward the Fermi level, explaining according to these authors the loss of stability in the latter compound. Our Ru:O COOP are mostly equivalent to the ones shown in the reference as well as the O:O one in RuO_3. The shape of the O:O COOP in Li_2RuO_3 is also correct, with the main anti-bonding peak at about 1 eV below the one in RuO_3.

3.4 V_2O_3

V_2O_3 is a Mott-Hubbard system showing a metal-insulator transition at approximately 150 K. The low temperature phase is monoclinic and anti-ferromagnetic and has been the subject of an intense debate to understand resonant x-ray diffraction (R-XRD) experiments performed to probe its magneto-electric structure. Using the data recorded by Paolasini and co-workers,[21] we have shown that orbital ordering is not observed and most of the signal is
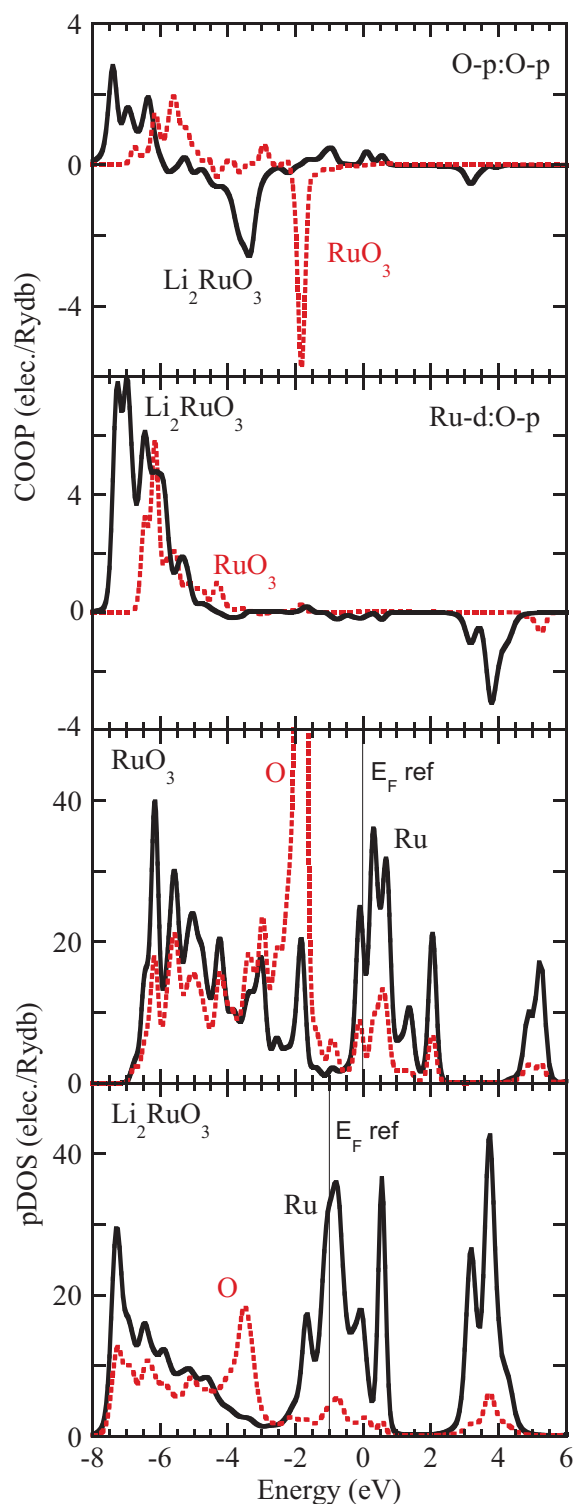
Figure 4: COOP and pDOS in RuO_3 and Li_2RuO_3. These simulations can be compared to Fig. 1 and 2 from the work by Saubanère *et al.*[7] Both the COOP (top) and the pDOS (bottom) have essentially the same shapes than in the reference. For Li_2RuO_3, we nevertheless obtain a 1 eV shift of the Fermi level. The position of the Fermi level of the reference is shown by a vertical line.

a pure magnetic phenomena. For this purpose, we used Bragg peaks with different in and out polarizations including cross channels ($\sigma - \sigma$, $\sigma - \pi$).[22]

Our interest here is to show that COOP simulation of magnetic systems are also possible. The simulations in Fig. 5 include spin-orbit interactions in the valence states, mandatory to probe magnetic contribution at the K-edges. We performed a self-consistent calculation using multiple scattering theory for a 5 Å radius cluster. In the unit cell, there are 8 equivalent vanadium atoms, each of them surrounded by a distorted octahedron. From the magnetic space group point of view there are two non-equivalent oxygen sites, labeled in the following by 2 and 3, but the COOP between the central vanadium and its six neighbors are formally different because the local punctual group has a symmetry of 1. Nevertheless, most features can be seen choosing two of them, prototypical of the 2 and 3 sites. Besides the good reproduction of the (1,1,1) reflection spectra, in both polarization channels $\sigma - \sigma$ and $\sigma - \pi$, we understand the pure dipole (E1E1) contribution is zero for this reflection. The intensity comes only for the dipole-quadrupole (E1E2) and the pure quadrupole (E2E2) channels, with different relative ratio depending on the azimuth. Here, the purpose is not to go in these details which are extensively studied in our previous paper,[22] but to correlate the spectral features with the calculated COOPs.

The data and simulation of absorption and diffracted peaks is introduced in Fig. 5 along with the pDOS for the vanadium and the two oxygen sites, and the COOP between them. Here, we show the contribution from both spin states to the signal. The up and down pDOS has evidently connections with COOP of the same spin states. For example the V-3d spin up peak at -1.5 eV correspond to the up O-3d:O-2p COOP. We note that it is bounding for one site and anti-bonding for the other one. The bonding or anti-bonding characters are the same for up and down states along the range probed by the R-XRD (1,1,1) reflection.
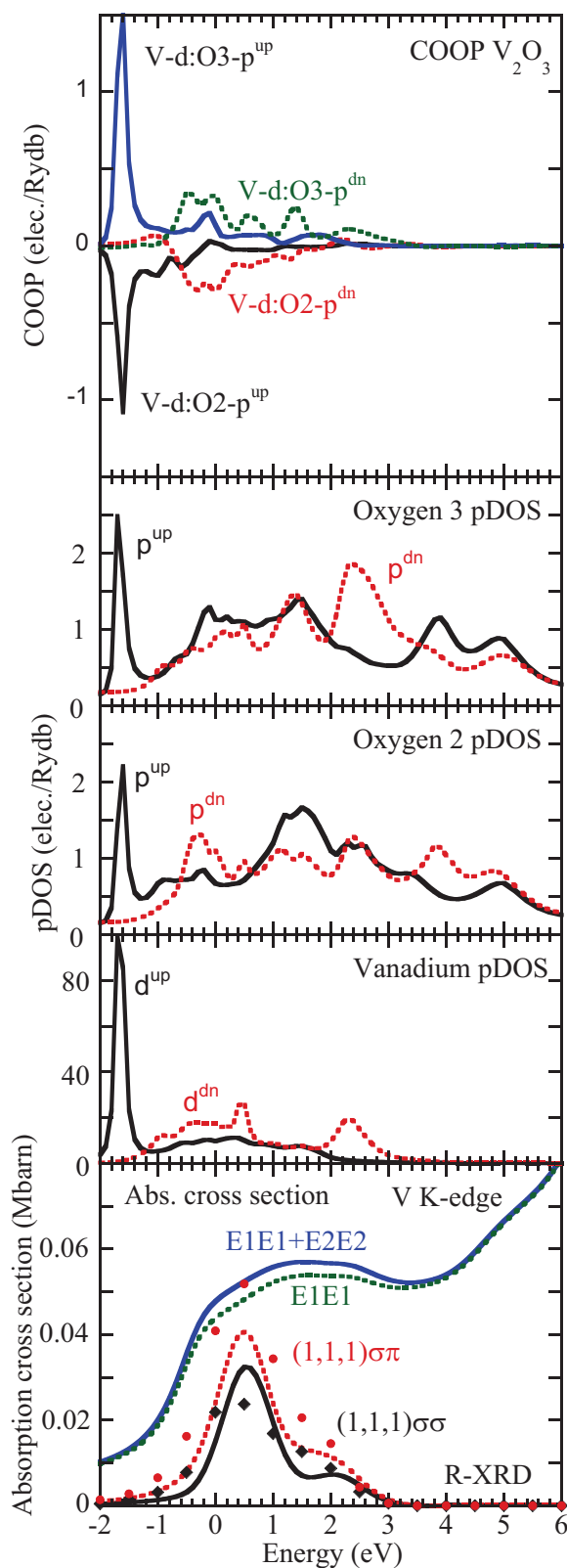
Figure 5: R-XRD and XANES at the V K-pre-edge, pDOS and COOP spectra in V_2O_3. Bottom: (1,1,1) reflection for 2 polarizations; data (points) by Paolasini *et al.*[21] shifted by 5465.5 eV; calculations (dotted and full lines), with also the XANES dipole (E1E1, dotted) and total (E1E1+E2E2, full line). Above: V, O2 and O3 sites pDOS. Top: V:O2 and V:O3 COOP. In this range, V-3*d*:O-2*p* is mainly bonding for O3 and anti-bonding for O2.
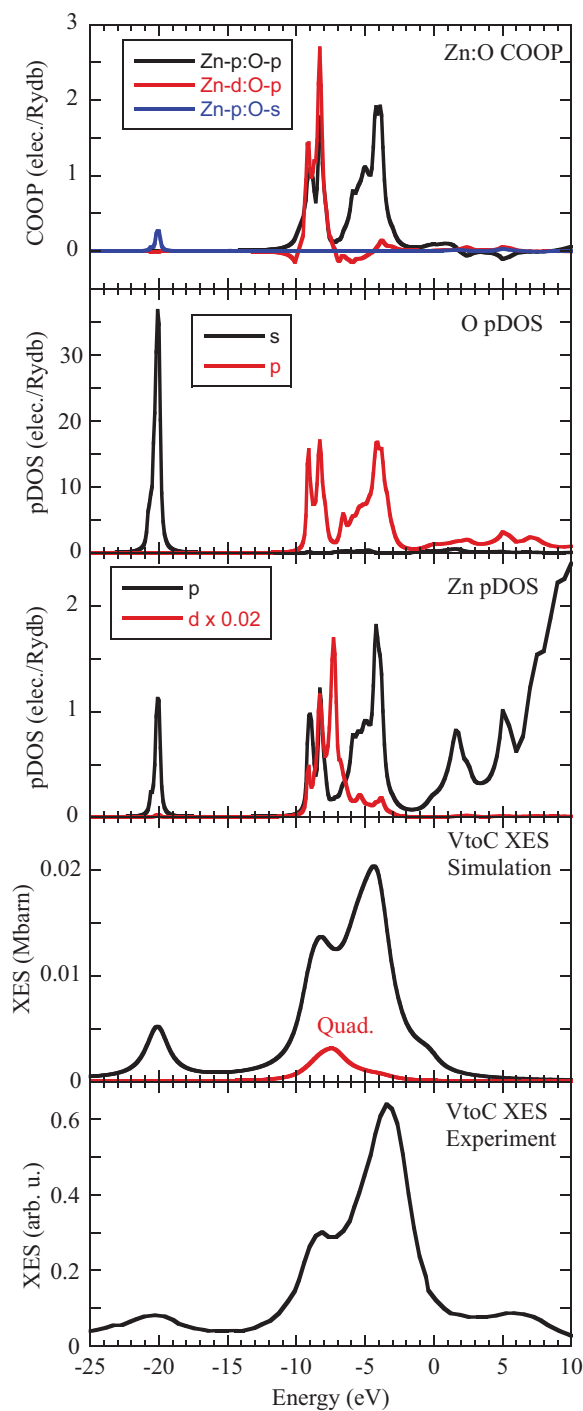
Figure 6: Valence to core XES at the Zn K-edge, pDOS and COOP spectra in ZnO. Bottom is the experiment by Gallo and Glatzel[23] shifted by 9659.5 eV to match the simulation just above where is shown the total XES and the quadrupole contribution. Then the pDOS for Oxygen and Zinc and top the COOP. The O-2s:Zn-4p COOP reveals the corresponding molecular orbital responsible of the experimental peak at -20 eV and explains the sensitivity of this spectroscopy to the nature of the ligand.

3.5 ZnO

The FDMNES code calculates also the valence to core (VtoC) x-ray emission spectroscopy (XES). This expression giving the emission cross-section is exactly the same that the one for XANES. In the mono-electronic approach, the difference between XES and XANES is that the cross section is proportional to the pDOS of the states below and above the Fermi level, respectively. The COOP calculation provides thus in the same way, the means to identify the features observed in the spectra in terms of molecular bonds, which have most often a bonding character at these energies below the Fermi level. To illustrate this, we take the example of a simple metal oxide, ZnO, with Zn K-edge VtoC XES recorded at ID26 (ESRF, France). It was already analyzed by Gallo and Glaztel,[23] using pDOS, and here we complete their work by the use of COOPs. We did self-consistent calculations in the ground state, with a 7 Å cluster radius. In the XES calculation, we have included the quadrupole term which probes the $3d$ states. In figure 6, we see the satisfactory agreement between experiment and simulation. The energy range close to the Fermi level is not perfectly reproduced, probably because of a multi-electronic response of the excited state. The three main features are nevertheless present and easily identified. Note that the calculation with the core hole, as it can be done in DFT, does not improve the spectra significantly. The figure also shows the pDOS of Zinc and Oxygen. Very evidently the Zn $4p$ DOS is nearly proportional to the XES cross section, but for the broadening that we have chosen with a constant width for simplicity. This one could be increased in the lower part of the energy range of the spectra, but without a convenient theoretical justification we prefer to keep it equal to the core-hole width all along the range. We can also check the correspondence between the Zn-$3d$ states and the quadrupolar contribution in the signal which is not negligible, but is not remarkable by a specific peak. On top of the figure the COOP is presented. The $4p$-Zn:$2p$-O is associated to the main VtoC-XES signal below the Fermi level. One also sees the correspondence between the $3d$-Zn:$2p$-O and the quadrupolar XES component. Here, the most significant feature is the $4p$-Zn:$2s$-O, because it is responsible of the peak at -20 eV. This feature, observable in

many oxides, is known to be a probe of the nature of the ligand. The energy of the $2s$ states strongly depends on the chemical species, and its amplitude on the bond length. The COOP gives a precise evaluation of all this, and can help to more precisely interpret the bonding of low symmetry sites.

4　Conclusion

We have presented a new tool to perform COOP calculations, which can be done together with XANES, valence to core XES, or resonant XRD spectral simulations. The different signs of COOP reveals the bonding or anti-bonding character of the molecular orbitals greatly simplifying the assignment of different features in the spectra in terms of specific bonds than when projected DOS on the atoms is used. Several examples have been introduced to demonstrate these simulations are precise fullfilling our expectations for known systems. We have also shown in more complex situations which need spin-orbit that different magnetic contributions in diffraction can be addressed in an anti-ferromagnetic system. The tool is now ready to handle most class of systems where X-ray spectroscopies are used to understand the bonding with the ligands. It is for example the case of the actinides where the role of the $5f$ states is debated.

Acknowledgement

References

(1) Bokhoven, J. A. V., Lamberti, C., Eds. *X-Ray Absorption and X-Ray Emission Spectroscopy*; John Wiley & Sons, Ltd: Chichester, West-Sussex, United Kingdom, 2016.

(2) Joly, Y.; Grenier, S. Theory of absorption near edge structure. In *X-Ray Absorption and X-Ray Emission Spectroscopy*; Bokhoven, J. A. V., Lamberti, C., Eds.; John Wiley & Sons, Ltd: Chichester, West-Sussex, United Kingdom, 2016; Chapter 4, pp 73–97.

(3) Nazarenko, E.; Lorenzo, J. E.; Joly, Y.; Hodeau, J.-L.; Mannix, D.; Marin, C. Resonant X-ray diffraction studies on the charge ordering in magnetite. *Phys. Rev. Lett.* **2006**, *97*, 056403.

(4) Dronskowski, R.; Bloechl, P. E. Crystal orbital Hamilton populations (COHP): energy-resolved visualization of chemical bonding in solids based on density-functional calculations. *The Journal of Physical Chemistry* **1993**, *97*, 8617–8624.

(5) Canadell, E.; Doublet, M.-L.; Iung, C. *Orbital Approach to the Electronic Structure of Solids*; Oxford University Press, Oxford, New York, 2012.

(6) Maintz, S.; Deringer, V. L.; Tchougréeff, A. L.; Dronskowski, R. LOBSTER: A tool to extract chemical bonding from plane-wave based DFT. *Journal of Computational Chemistry* **2016**, *37*, 1030–1035.

(7) Saubanère, M.; McCalla, E.; Tarascon, J.-M.; Doublet, M.-L. The intriguing question of anionic redox in high-energy density cathodes for Li-ion batteries. *Energy Environ. Sci.* **2016**, *9*, 984–991.

(8) Bunău, O.; Joly, Y. Self-consistent aspects of x-ray absorption calculations. *J. Phys.: Condens. Matter* **2009**, *21*, 345501.

(9) The code can be downloaded at the web address: www.neel.cnrs.fr/fdmnes.

(10) Bunău, O.; Joly, Y. Time-dependent density functional theory applied to x-ray absorption spectroscopy. *Phys. Rev. B* **2012**, *85*, 155121, The code.

(11) Guda, S. A.; Guda, A. A.; Soldatov, M. A.; Lomachenko, K. A.; Bugaev, A. L.; Lamberti, C.; Gawelda, W.; Bressler, C.; Smolentsev, G.; Soldatov, A. V.; et al, Finite

difference method accelerated with sparse solvers for structural analysis of the metal-organic complexes. *J. Phys.: Conf. Ser.* **2016**, *712*, 012004.

(12) Joly, Y. X-ray absorption near-edge structure calculations beyond the muffin-tin approximation. *Phys. Rev. B* **2001**, *63*, 125120.

(13) Wood, J. H.; Boring, A. M. Improved Pauli Hamiltonian for local-potential problems. *Phys. Rev. B* **1978**, *18*, 2701–2711.

(14) Laffon, C.; Ehrke, H.; Parent, P.; Wurth, W.; Tourillon, G. MS-X approach of near edge X-ray absorption spectra of the acrylonitrile molecule (CH2CHCN). *Physica B: Condensed Matter* **1995**, *208-209*, 56 – 58, Proceedings of the 8th International Conference on X-ray Absorption Fine Structure.

(15) Parent, P.; Laffon, C.; Tourillon, G.; Cassuto, A. Adsorption of Acrylonitrile on Pt(111) and Au(111) at 95 K in the Monolayer and Multilayer Ranges Studied by NEXAFS, UPS, and FT-IR. *The Journal of Physical Chemistry* **1995**, *99*, 5058–5066.

(16) Joly, Y. Calculating X-ray absorption near-edge structure at very low energy. *Journal of Synchrotron Radiation* **2003**, *10*, 58–63.

(17) Poumellec, B.; Cortes, R.; Tourillon, G.; Berthon, J. Angular Dependence of the Ti K Edge in Rutile TiO2. *physica status solidi (b)* **1991**, *164*, 319–326.

(18) Joly, Y.; Cabaret, D.; Renevier, H.; Natoli, C. R. Electron Population Analysis by Full-Potential X-Ray Absorption Simulations. *Phys. Rev. Lett.* **1999**, *82*, 2398–2401.

(19) Kobayashi, H.; Kanno, R.; Kawamoto, Y.; Tabuchi, M.; Nakamura, O.; Takano, M. Structure and lithium deintercalation of Li2xRuO3. *Solid State Ionics* **1995**, *82*, 25 – 31.

(20) Akimoto, J.; Gotoh, Y.; Oosawa, Y. Synthesis and Structure Refinement of LiCoO2Single Crystals. *Journal of Solid State Chemistry* **1998**, *141*, 298 – 302.

24

(21) Paolasini, L.; Matteo, S. D.; Vettier, C.; de Bergevin, F.; Sollier, A.; Neubeck, W.; Yakhou, F.; Metcalf, P.; Honig, J. Interplay between orbital and magnetic long range order by resonant X-ray scattering in (V1xCrx)2O3. *Journal of Electron Spectroscopy and Related Phenomena* **2001**, *120*, 1 – 10.

(22) Joly, Y.; Di Matteo, S.; Natoli, C. R. Ab initio simulations of resonant x-ray scattering on the insulating phase of V_2O_3 compared with recent experiments. *Phys. Rev. B* **2004**, *69*, 224401.

(23) Gallo, E.; Glatzel, P. Valence to Core X-ray Emission Spectroscopy. *Advanced Materials* **2014**, *26*, 7730–7746.